Journal of
Applied Remote Sensing

RemoteSensing.SPIEDigitalLibrary.org

Self-adaptive block-based compressed sensing imaging for remote sensing applications

Xiao-Dong Wang
Yun-Hui Li
Zhi Wang
Wen-Guang Liu
Dan Liu
Jia-Ning Wang

SPIE.

Xiao-Dong Wang, Yun-Hui Li, Zhi Wang, Wen-Guang Liu, Dan Liu, Jia-Ning Wang, "Self-adaptive block-based compressed sensing imaging for remote sensing applications," *J. Appl. Remote Sens.* **14**(1), 016513 (2020), doi: 10.1117/1.JRS.14.016513

Self-adaptive block-based compressed sensing imaging for remote sensing applications

Xiao-Dong Wang,[a] Yun-Hui Li,[a,b,*] Zhi Wang,[a,c] Wen-Guang Liu,[a] Dan Liu,[a,b] and Jia-Ning Wang[a,b]

[a]Chinese Academy of Sciences, Changchun Institute of Optics, Fine Mechanics and Physics, Changchun, China

[b]University of Chinese Academy of Sciences, Beijing, China

[c]Changchun UP Optotech (Holding) Co., Ltd., Changchun, China

Abstract. In order to effectively alleviate the pressure of high-resolution imaging and massive data storage and transmission, it is of great practical significance to introduce compressed sensing into remote sensing applications. From the perspective of imaging control strategy, the typical block-based compressed sensing (BCS) system is optimized. Based on the fact that there are generally significant differences between regions of remote sensing images, a self-adaptive BCS method is proposed. Compared with the traditional BCS system, the prior information of the imaging target is obtained first by adding a presampling process. On the one hand, it is used to generate a saliency information map, which guides the reasonable allocation of self-adaptive sampling ratios between blocks in the compressed sampling process, thereby improving the sampling efficiency. On the other hand, it is used to generate the weighted sparse coefficient matrix, which will be substituted into the theoretical model in the image restoration process, thus improving the image restoration efficiency. The experimental results show that the imaging quality of the proposed method has a significant improvement compared with the traditional system and is also superior to several existing self-adaptive methods. In addition, on the basis of the above method, a multiangle image restoration strategy is proposed, which further improves the image quality at the cost of four times the image restoration time. [DOI: 10.1117/1.JRS.14.016513]

Keywords: compressed sensing; self-adaptive; remote sensing.

Paper 190625 received Aug. 15, 2019; accepted for publication Feb. 11, 2020; published online Mar. 3, 2020.

1 Introduction

The compressed sensing theory developed in the recent years has challenged the traditional cognition in the field of signal processing. It specifies that, based on the sparse property, the original signal can be accurately restored from a small number of linear projections with high probability, which breaks the constraint of Nyquist–Shannon sampling theorem.[1–6] This theory provides a new way to address the growing pressure in the field of signal processing. It has shown great potential in reducing the performance requirements for sampling devices, reducing the amount of sampling data, and thereby alleviating the pressure on data storage and transmission. Therefore, it has attracted wide attention in various fields, including data compression,[7,8] medical imaging,[9–12] radar,[13,14] three-dimensional imaging,[15] super-resolution imaging,[16,17] and remote sensing imaging.[18,19]

With the gradual improvement of temporal resolution, spatial resolution, and spectral resolution, the amount of data generated by remote sensing imaging systems has increased dramatically, which seriously conflicts with the limited on-board storage and data transmission bandwidth. Therefore, it is of great practical significance to introduce compressed sensing into remote sensing applications. As a typical application of compressed sensing theory in imaging systems, Duarte et al.[20] pioneered a single-pixel camera, which realized compressed sensing

*Address all correspondence to Yun-Hui Li, E-mail: liyunhui_ciomp@126.com

1931-3195/2020/$28.00

imaging based on the digital micromirror device. The single-pixel design reduces the photodetector array down to a single unit. However, with the expansion of imaging scale, the number of sampling increases dramatically, resulting in a sharp increase in sampling time. In the meantime, the computational complexity of image restoration has also risen steeply due to the growing matrix size. In order to alleviate the above problems, a block-based compressed sensing (BCS) system is proposed, which decomposes the target image into several blocks and then performs parallel compressed sensing on each sub-block. Parallel processing reduces the sampling time and the computational complexity of image restoration, which improves the real-time performance of the imaging system.[21–23]

At present, the research on BCS imaging systems mainly focuses on two parts: one is the improvement of theoretical models, and the other is the optimization of imaging control strategies. The research on theoretical models includes the improvement of measurement matrix, sparse transform base, and restoration algorithm, which involves both single-parameter improvement and multiparameter collaborative improvement. Gan[24] proposed a BCS framework for natural images, which offered a fast, good initial solution at the receiver side by using linear minimum mean-square-error estimation. A deep neural network approach to BCS was proposed by Adler et al.,[25] in which the measurement matrix and the nonlinear reconstruction operator were jointly optimized during the training phase. Coluccia et al.[26] proposed a method to enforce smoothness across block borders by modifying the sensing and reconstruction process so as to employ partially overlapping blocks. In order to achieve a better reconstruction performance for aerial imagery, Liu et al. proposed the adaptive-thresholding projected Landweber reconstruction algorithm that leveraged the piecewise-linear thresholding model for wavelet-based image denoising.[27] Yang and Lin[28] proposed a variation-based block compressed sensing restoration method, which decomposed the image into several nonoverlapping blocks first, followed by the scanning according to the column and measurement by blocks, so as to obtain several column vectors of measurement value. A BCS scheme with matrix permutation was proposed by Zhang et al.,[29] which could be utilized to encode natural images effectively. Zhou et al. proposed a collaborative BCS framework with dual-domain sparse representation, where local structural information and nonlocal pixel similarity were jointly considered.[30]

Based on the characteristics of the BCS imaging system, the research on imaging control strategies is mainly to complete the optimal allocation of sampling resources, thereby maximizing the imaging quality. In the traditional BCS system, the same sampling ratio and measurement matrix are usually shared for different blocks of the imaging target without distinction. However, the richness of the information contained in each region is inevitably different from each other, thus resulting in a difference in compressibility. This indiscriminate processing method results in the waste of compressed sampling resources and image restoration resources, which should be exactly the advantage of compressed sensing imaging compared with traditional imaging. Therefore, how to quantify the compressibility of different blocks in the target image, and then to replan the allocation of imaging system resources is an important research content, which is called self-adaptive compressed sensing.

In recent years, the application research of self-adaptive BCS in imaging systems is mainly manifested in two aspects: one is image data compression, the other is compressed sensing imaging, and more research focuses on the former. The characteristics of image compression are: on the one hand, it is convenient to extract prior information because the image to be compressed is known, on the other hand, image compression is mainly embodied in mathematical algorithms, which is less constrained by hardware and easier to implement. A self-adaptive sampling and reconstruction algorithm for BCS is presented in Ref. 31, in which the sampling ratio is assigned depending on its texture complexity of each block.[31] Wang et al. proposed a self-adaptive sampling method. The spacial frequency is utilized to extract the textural features of image blocks, and then each block is categorized into the smooth blocks or the textual blocks. To the textural blocks, the sampling ratio is modified adaptively by combing with the statistical characteristics of the coefficients in wavelet domain.[32] Zhu et al. applied a self-adaptive sampling mechanism to the reweighted BCS. The proposed self-adaptive sampling allocates the measurements to each image block according to the statistical information so as to sample and restore the image more efficiently.[33] A reweighted compressed sampling for image compression was proposed by Yang et al. It introduces a weighting scheme into the traditional compressed sensing

framework whose coefficients are determined in encoding side according to the statistics of image signals.[34] Zhirong Gao et al. proposed two image compression methods. One is called coefficient random permutation (CRP), and the other is termed adaptive sampling (AS). The CRP method can be effective in balancing the sparsity of sampled vectors in discrete cosine transform (DCT) domain of the image, thus improving the sampling efficiency. The AS is achieved by designing a self-adaptive measurement matrix based on the energy distribution characteristics of the image in DCT domain, which has a good effect in enhancing the performance.[35] A jointly reweighted BCS scheme was developed by Zhu. By applying weighting factors to the image data and sampling matrix simultaneously, the weighting efficiency of the traditional reweighted BCS scheme is improved.[36] Xu et al.[37] proposed a perceptual rate-distortion optimized compressed sensing image codec to achieve a maximal perceptual quality.

Compared with image compression, compressed sensing imaging is constrained by the fact that the prior information of the imaging target cannot be obtained before imaging, and the compressed sensing process needs to be implemented with the help of hardware. However, it not only relieves the pressure on the detector and the front-end analog-to-digital sampling device in the remote sensing system but also effectively reduces the amount of sampling data. These advantages are not all available for image compression. Considering the similarity of the structure contained in the image blocks, a simple but efficient self-adaptive structured compressed sensing was proposed by Zhang. The proposed measurement matrix consists of two submatrices. The premeasurement matrix aims to estimate the compressibility of the image blocks and ensure the minimal measurements for restoration. The self-adaptive measurement matrix is relatively flexible and depends on the compressibility estimated.[38] Yu et al. proposed a saliency-based compressed sampling scheme for image signals. The key idea is to exploit the saliency information and allocate more sampling resources to salient regions but fewer to nonsalient regions. To obtain the saliency information, they provided a saliency generation model, which employed a low-resolution complementary sensor to acquire a sample image of the target.[39] Based on the fact that low-frequency components are relatively more crucial to the perceptual quality of images than high-frequency components, Yang et al. proposed a novel sampling scheme for compressed sensing by designing a weighting scheme for the measurement matrix. By adjusting the weighting coefficients, they can tune the structure of the measurement matrix to favor the frequency components that are important to human perception so that those components could be more precisely restored in the restoration procedure. For two-dimensional (2-D) DCT, a convenient way is to derive the weighting coefficients from JPEG quantization table by taking the inverse of the table entries and adjusting their amplitudes to a proper range.[40]

Based on the above research status, a self-adaptive block-based method for remote sensing imaging is proposed in this paper, which adopts self-adaptive processing in both compressed sampling and image restoration. Compared with the traditional BCS system, the prior information of the imaging target is obtained first by adding presampling process. On the one hand, it is used to generate a saliency information map, which guides the reasonable allocation of self-adaptive sampling ratios between blocks in the compressed sampling process, thereby improving the sampling efficiency. On the other hand, it is used to generate the weighted sparse coefficient matrix, which will be substituted into the theoretical model in the image restoration process, thus improving the image restoration efficiency.

Compared with the current existing methods, the advantages of the method proposed in this paper are as follows.

a. This method is implemented on the basis of the original BCS architecture without increasing the hardware complexity.
b. In the process of compressed sampling, a presampling stage for obtaining prior information is added. The presampled data are used to extract image features while also being used for image restoration without causing a waste of sampling resources.
c. Based on the prior information extracted from the presampled data, self-adaptive algorithms are adopted in the process of compressed sampling and image restoration simultaneously, so the final imaging quality is superior to the current variety of self-adaptive methods, which adopt self-adaptive algorithm only in one of the above two processes.

The structure of this paper is organized as follows: Section 2 introduces the typical BCS theory model and its corresponding imaging system. The self-adaptive BCS imaging method proposed in this paper is elaborated in Sec. 3, which includes two parts of self-adaptive compressed sampling and self-adaptive image restoration. In Sec. 4, we proposed the multiangle integrated image restoration strategy. Based on the proposed self-adaptive BCS method and image restoration strategy, the working path of image restoration process is combed in Sec. 5. The experimental verification and result analysis are presented in Sec. 6. After summarizing the above contents, the conclusions are given in Sec. 7.

2 Block-Based Compressed Sensing

2.1 *Block-Based Compressed Sensing Theory Model*

It is assumed that the imaging target can be divided into B blocks, each of which has a size of $r \times c$. When the number of compressed sampling for each block is m, the whole compressed sensing process can be expressed as

$$Y^b = \Phi^b X^b = \Phi^b \Psi \Theta^b = \Lambda^b \Theta^b \qquad (b = 1 \ldots B), \tag{1}$$

where b is the ordinal number of each block. For any block b, $Y^b \in \mathbb{R}^{(r \cdot c)}$ is the measurement result vector, $\Phi^b \in \mathbb{R}^{m \times (r \cdot c)}$ is the measurement matrix, $\Theta^b \in \mathbb{R}^{(r \cdot c)}$ is the sparse representation of the target signal vector $X^b \in \mathbb{R}^{(r \cdot c)}$ under the sparse basis $\Psi \in \mathbb{R}^{(r \cdot c) \times (r \cdot c)}$, and $\Lambda^b = \Phi^b \Psi$ is called the sensing matrix. Each element in the vector X^b corresponds to the gray value of one pixel in the target image.

For any block b, the sparse coefficient vector $\hat{\Theta}^b$ can be obtained based on the measurement result matrix Y^b by solving the optimization problem shown in the following equation:

$$\hat{\Theta}^b = \arg\min_{\Theta^b \in \mathbb{R}^N} \|\Theta^b\|_{\ell 1} \quad \text{subject to } Y^b = \Lambda^b \Theta^b \quad (b = 1 \ldots B). \tag{2}$$

Further, the restored image $\hat{X}^b = \Psi \Theta^b$ of each block can be obtained, and then all the blocks are integrated into a complete restored image.

2.2 *Block-Based Compressed Sensing Imaging System*

As shown in Fig. 1, the typical BCS imaging system is mainly composed of optical lenses, a coded aperture, and an area array detector. The imaging target is first incident on the coded aperture template through the front-end optical lens, and then the encoded optical signal is

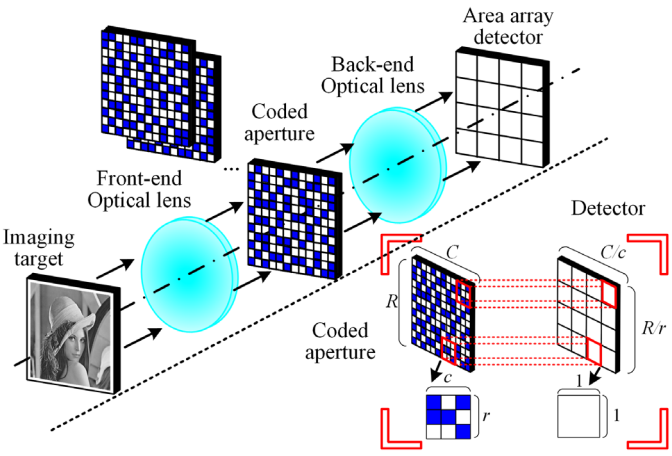

Fig. 1 The composition of BCS imaging system.

incident on the detector through the back-end optical lens. There is a strict correspondence between the detector and the encoded template. One detector pixel corresponds to the encoded template with the size of $r \times c$, and the pixel number of the detector corresponds to the number of image blocks.

Taking any block b in the actual imaging system as an example, assuming that the imaging target is $G^b \in \mathbb{R}^{r\times c}$, the measurement result is Y^b, and the coded aperture template is $C(p)^b \in \mathbb{R}^{r\times c}(p = 1 \ldots m)$, in which p represents the p'th coded sampling, then the whole compressed sensing process can be expressed as

$$Y^b_{p,1} = \mathrm{sum}(G^b .\times C(p)^b) \qquad (p = 1 \ldots m, b = 1 \ldots B), \tag{3}$$

where $\mathrm{sum}(\cdot)$ means the sum operation of each element in the matrix, and $Y^b_{i,j}$ represents the i'th row and j'th column element of the measurement result matrix Y^b.

The elements in the measurement matrix Φ^b can be organized as follows:

$$\Phi^b_{p,(i-1)\times c+j} = C(p)^b_{i,j} \qquad \begin{array}{l}(i = 1 \ldots r, j = 1 \ldots c)\\ (p = 1 \ldots m, b = 1 \ldots B)\end{array} \tag{4}$$

The elements in the signal matrix X^b to be measured are organized as follows:

$$X^b_{(i-1)\times c+j} = G^b_{i,j} \qquad (i = 1 \ldots r, j = 1 \ldots c). \tag{5}$$

3 Self-Adaptive Block-Based Compressed Sensing Imaging Method

3.1 *Overall Composition of the Method*

The imaging flow of traditional compressed sensing imaging method is shown in the solid frame part of Fig. 2, which can be divided into two stages: compressed sampling and image restoration. In contrast, the self-adaptive method proposed in this paper adds presampling process to the compressed sampling stage, and then the priori information extracted by presampling can guide the subsequent self-adaptive compressed sampling and image restoration process so that a higher quality image can be acquired, as shown in the dotted frame part of Fig. 2.

It can be seen from the figure that the proposed method includes two processes: self-adaptive compressed sampling and self-adaptive image restoration. Both of them will be elaborated separately below.

3.2 *Self-Adaptive Compressed Sampling*

3.2.1 *Compressed sampling method*

Due to the pressure of massive image data storage and transmission, as well as the constraints imposed by the system hardware and application environment, there is usually a certain sampling ratio limitation in the practical application of compressed sensing system. For traditional BCS imaging systems, the average allocation of sampling resources is usually adopted, that is, the same sampling ratio is used for each block of the imaging target without discrimination. However, for actual images, especially for remote sensing images, there are bound to be

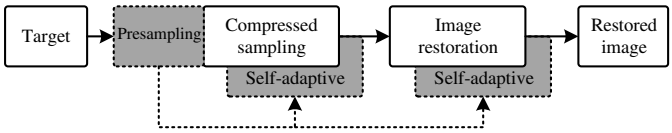

Fig. 2 The imaging flowchart of self-adaptive compressed sensing imaging method.

differences in the richness of feature information between regions, which results in unreasonable allocation of sampling resources, thus limiting the improvement of imaging quality.

Based on this, we propose a self-adaptive compressed sampling method. First, the feature information map of the imaging target is extracted based on the presampled data, and then it is used as the weight value of different blocks to guide the reasonable allocation of compressed sampling resources, so as to improve the compressed sampling efficiency.

Figure 3 shows the schematic diagram of self-adaptive compressed sampling. The compressed sampling process can be divided into three stages: presampling, basic sampling, and additional sampling. The number of presampling and basic sampling are equally allocated by each block, and both of them are preset values. The additional samplings of each block are obtained based on a specific algorithm. There is a problem of limited channel capacity in remote sensing imaging system, so it is necessary to calculate the average sampling ratio based on the data bandwidth and imaging scale, and then the total samplings can be obtained. After being allocated to the presampling and basic sampling, respectively, the remaining will be reserved for additional sampling. In the presampling stage, the low-resolution image is obtained directly by uncompressed sampling. Based on this image, saliency information map can be generated, and then it will be used to generate the sampling allocation results of each block in the additional sampling stage.

The lower part of Fig. 3 shows the workflow of self-adaptive compressed sampling, in which the saliency information map generation based on presampled data and the sampling allocation strategy are executed in parallel with the basic sampling to ensure the continuity of the sampling process.

Unlike the compressed sampling method used in basic sampling and additional sampling, presampling adopts the uncompressed sampling method instead, and the specific implementation is shown in Fig. 4. Assuming that the size of any block in the BCS system is $r \times c$, and it can be redivided into $r/l \times c/q$ parts in the case that each $l \times q$ is integrated into one part, which can be used as the encoding unit for uncompressed sampling. The presampling process can be expressed as

$$Y' = \Phi' \cdot X' = I \cdot X' = X', \tag{6}$$

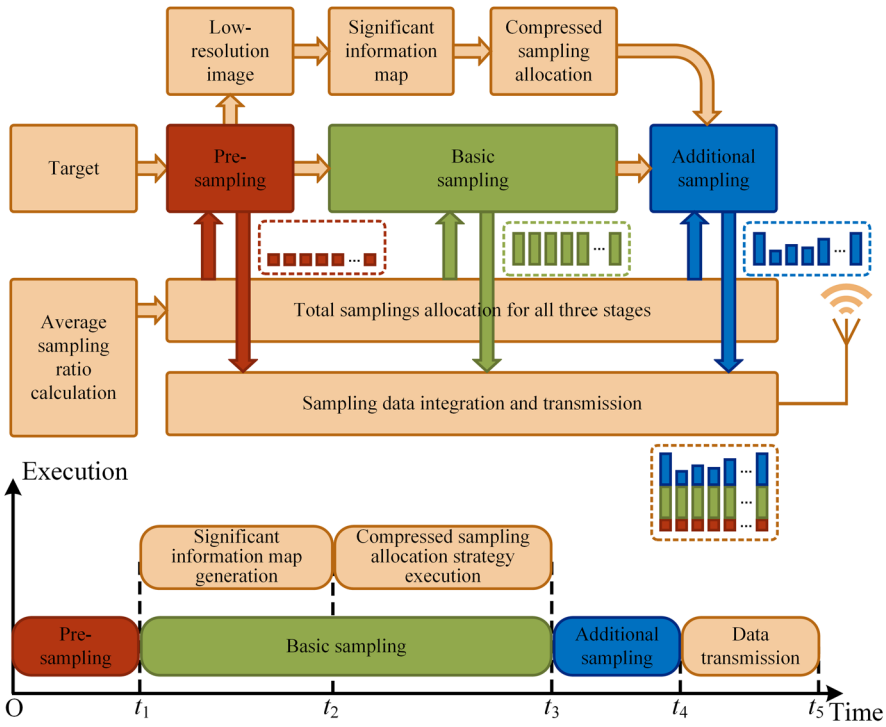

Fig. 3 The schematic diagram of self-adaptive compressed sampling.

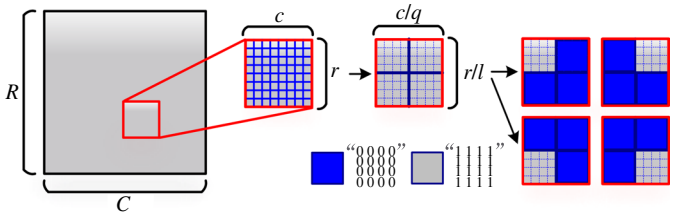

Fig. 4 The schematic diagram of uncompressed sampling in the presampling stage.

where Φ' is the measurement matrix, X' is the target image, and Y' is the sampling result. Since Φ' is the unit matrix, there is $Y' = X'$, that is, the sampling result is the low-resolution version of the imaging target, and no image restoration is required.

It should be noted here that although the presampling takes up a small amount of sampling resources, the sampling data are effectively utilized, which is manifested in three aspects. First, it is used to generate a saliency information map to guide the self-adaptive sampling process. Second, the weight coefficient matrix used for image restoration is generated to guide the self-adaptive image restoration process. Third, as a part of the sampling process, it can also be treated as valid sampling data for a subsequent image restoration process. As the key components of the self-adaptive sampling process, saliency information map generation and self-adaptive compressed sampling allocation strategy will be described in detail below.

3.2.2 *Saliency information map generation*

As shown in Fig. 5, based on the low-resolution image acquired by presampling, a high-resolution image with the same resolution as the imaging target is first generated by bilinear interpolation, and then the saliency information map is extracted with the help of a specific algorithm.

There are various algorithms for extracting saliency information maps, including sign function algorithm, variance algorithm, significant coefficient algorithm, and texture feature algorithm. These algorithms will be described separately below.

Sign function algorithm. Given the target image X, the saliency information map F can be calculated by the following equations:[39]

$$\begin{aligned} P &= \text{sign}[C(X)] \\ S &= \text{abs}[C^{-1}(P)] \\ F &= G * S^2, \end{aligned} \tag{7}$$

where $C(\cdot)$ and $C^{-1}(\cdot)$ represent the 2-D DCT and its inverse transform, respectively. $\text{sign}(\cdot)$ is a sign function, $\text{abs}(\cdot)$ is an absolute value function, and G is a 2-D Gaussian low-pass filter.

Variance algorithm. Variance is usually a simple and effective criterion for evaluating the richness of information contained in an image. The larger the variance is, the richer the information contained in the image is. Therefore, the weighting factor $f(i)$ of each block can be obtained by calculating the variance σ_i^2 so that it can be combined to form a saliency information map:

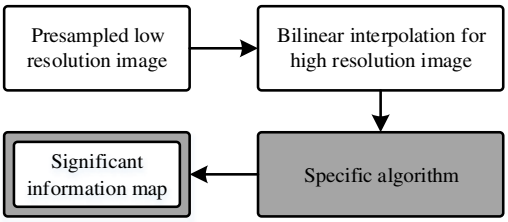

Fig. 5 The process of generating saliency information map.

$$f(i) = \sigma_i^2 = \frac{1}{r \times c} \sum_{j=0}^{r \times c - 1} (b_j - \mu_i)^2, \tag{8}$$

where i is the ordinal number of the block with a size of $r \times c$. For any block, b_j represents the gray value of the j'th pixel, and μ_i represents the average gray value of all pixels in the block.

Significant coefficient algorithm. The number of significant coefficients in the sparse transform domain also indirectly represents the information content of the image. Therefore, the sparse matrix is first obtained by 2-D DCT of each block, and then the number of coefficients whose absolute value is higher than the preset threshold T is taken as the weighting factor of the block:

$$\begin{aligned} &\text{for } j = 1 : r \times c \\ &\quad \text{if } |\theta_j| \geq T \\ &\quad\quad s = s + 1 \\ &\quad \text{end} \\ &\text{end} \end{aligned} \tag{9}$$

where θ_j represents the j'th element of the sparse matrix transformed by 2-D DCT, and the final result s will be used as the weighting factor of the block.

Texture feature algorithm. The texture information can be obtained by directly comparing the differences between pixels, and then the information content of the image can be determined. The calculation of texture information can be expressed as

$$\begin{aligned} f(i) &= \sqrt{R_i^2 + C_i^2} \\ R_i &= \sqrt{\frac{1}{r \times c} \sum_{m=1}^{r} \sum_{n=2}^{c} [X(m,n) - X(m,n-1)]^2} \\ C_i &= \sqrt{\frac{1}{r \times c} \sum_{m=2}^{r} \sum_{n=1}^{c} [X(m,n) - X(m-1,n)]^2}, \end{aligned} \tag{10}$$

where i is the ordinal number of the block with a size of $r \times c$, $X(m,n)$ represents the gray value in the position of m'th row and n'th column of the block. The calculated result $f(i)$ represents the texture information and thus serves as the weighting factor of the i'th block.

3.2.3 *Compressed sampling allocation strategy*

The implementation of compressed sampling allocation strategy requires two important input conditions. One is the saliency information map generated by the above algorithms, which serves as the weight for self-adaptive sampling allocation. The other is the average sampling ratio available for self-adaptive allocation, which is calculated based on the system data bandwidth and imaging scale.

In all three sampling stages, the selection principle of presampling times is to extract more image feature information with minimal impact on the whole sampling process. The basic sampling times are determined by a prior estimation on the execution time of saliency information map generation and sampling allocation strategy. There is also a restriction on the maximum and minimum sampling times. The maximum sampling times are limited by the maximum coding time allowed by the system, and the minimum sampling times should not be less than the sum of presampling and basic sampling times.

The specific implementation process of the sampling allocation strategy is organized as in Algorithm 1.

Algorithm 1 Compressed sampling allocation strategy.

Task: Calculating the sampling ratio allocation for each block based on system parameters.

Input parameters:

- The imaging scale is $R \times C$, and it is divided into B blocks, each of which has a size of $r \times c$.
- The data channel capacity is Mbps, the maximum encoding time allowed for single image acquisition is T, and the sampling rate is v.
- The execution time of saliency information map generation and sampling allocation strategy is t, and $f(i)$ represents the weight of each block, which is extracted from saliency information map.

Initialization:

- Calculating the average compressed sampling ratio D_{av} in the case of 8-bit imaging depth:

$$\frac{(R \times C) \cdot D_{\text{av}}}{T} = M/8 \Rightarrow D_{\text{av}} = \frac{M \cdot T}{8 \cdot (R \times C)} \quad (0 < D_{\text{av}} < 1).$$

- Calculating the initial minimum sampling ratio $D_{\min}$.

  Calculating the sampling ratio D_{p+b} in the presampling and basic sampling stages:

$$D_{p+b} = \frac{vt}{r \times c}.$$

  The minimum sampling ratio $D_{\min}$ should be no less than D_{p+b}.

- Calculating the maximum sampling ratio $D_{\max}$:

$$D_{\max} = \begin{cases} 1 & (vT \geq r \times c) \\ \frac{vT}{r \times c} & (vT \leq r \times c) \end{cases}.$$

Main Iteration:

- Step 1: Calculating the initial sampling ratio D_i

$$D_i = \frac{f(i)}{\sum_{i=1}^{B^2} f(i)} \cdot D_{\text{av}} \cdot B \cdot k,$$

  where k is the adjustment factor during the iteration process, and its initial value is set to 1.

- Step 2: Limiting the range of parameter D_i

$$D_i = \begin{cases} D_{\min} (D_i \leq D_{\min}) \\ D_{\max} (D_i \geq D_{\max}) \\ D_i (D_{\min} < D_i < D_{\max}) \end{cases}.$$

- Step 3: Reviewing the actual sampling ratio D'_{av}

$$D'_{\text{av}} = \frac{1}{B} \sum_{i=1}^{B} D_i.$$

- Step 4: Updating adjustment variables

$$\begin{cases} k = k \cdot (1 + \Delta) \\ D_{\min} = D_{\min} \cdot (1 + \Delta) \end{cases},$$

  where $\Delta = D_{\text{av}} = D'_{\text{av}}$. If $|\Delta| \leq 1 \times 10^{-3}$, the iteration is terminated, otherwise, it will return to step 1 and continue the iteration until $|\Delta| \leq 1 \times 10^{-3}$.

Outputs: The sampling ratio D_i for each block in the imaging target.

3.3 *Self-Adaptive Image Restoration*

3.3.1 *Image restoration method*

The basic idea of self-adaptive image restoration is: first, based on the low-resolution image acquired in the presampling stage, the weight coefficient matrix of each block is extracted separately. Second, it is introduced into the theoretical model of compressed sensing, which is equivalent to weighting the elements representing different frequency components in the sparse matrix, thus realizing the self-adaptive image restoration. As a result, the efficiency of image restoration algorithm is improved for a better image quality.

Figure 6 shows the schematic diagram of self-adaptive image restoration. The weight coefficient matrix extracted from presampled data will be introduced into the image restoration process, and the theoretical model of compressed sensing with weight coefficient matrix can be expressed as follows:

$$Y = \Phi X = \Phi\Psi\theta = \Phi\Psi W\theta', \tag{11}$$

where the weight coefficient matrix W is a diagonal matrix, and the elements on the diagonal are weight values for different frequency components. Compared with the nonweighted processing, this method can increase the weight of low-frequency components, where the image information is mainly concentrated, thereby reducing the restoration error.

The image restoration is performed according to the improved model described above, wherein the presampled, basic sampled, and additional sampled data are all used for the sampling result matrix, so the measurement matrix in the above model can be expressed as

$$\Phi = \begin{bmatrix} \Phi_p \\ \Phi_b \\ \Phi_a \end{bmatrix}. \tag{12}$$

The measurement matrix Φ consists of three parts: Φ_p, Φ_b, and Φ_a, where Φ_b and Φ_a are the measurement matrices corresponding to the basic sampling and additional sampling, respectively, which are random matrices, and Φ_p represents the measurement matrix corresponding to the presampling, which is a deterministic matrix. According to the schematic diagram of uncompressed sampling process shown in Fig. 4, in the case that the size of each image is 8×8 and the number of presampling is 4, the form of the measurement matrix Φ_p is shown in Fig. 7.

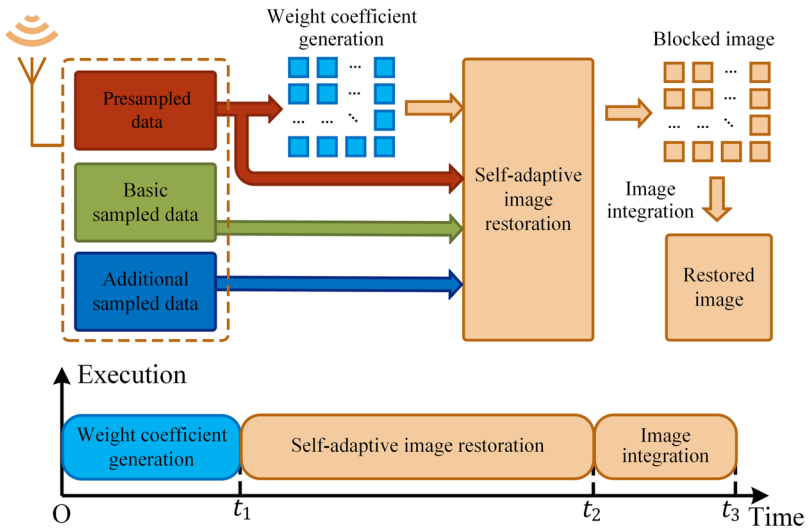

Fig. 6 The schematic diagram of self-adaptive image restoration.

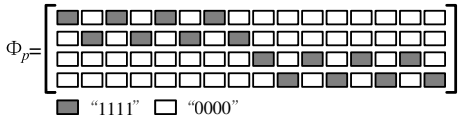

Fig. 7 The measurement matrix corresponding to the presampling stage.

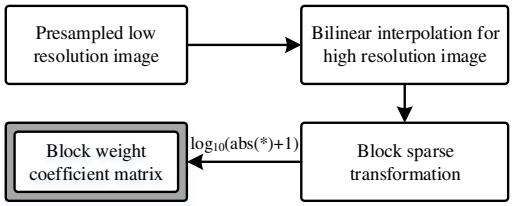

Fig. 8 The process of generating weight coefficient matrix.

The lower part of Fig. 6 shows the workflow of self-adaptive image restoration, in which the weight coefficient matrix generation, the block image restoration, and the image integration are performed in series.

3.3.2 *Weight coefficient generation*

The weight coefficient matrix proposed in Ref. 40 is derived from the quantization table used in the standard JPEG image compression format, whose advantage is that the matrix is determined and no real-time calculation is required. However, just because of this, it generally works well for all types of images, but it is not optimal for a specific type of image, such as remote sensing images. Moreover, the standard quantization table is based on DCT, which makes DCT the only choice for sparse transformation.

In this paper, the low-resolution image acquired in the presampling stage contains *a priori* feature information, which can be directly used to generate the weight coefficient matrix suitable for the current image, and this is undoubtedly optimal.

The process of generating weight coefficient matrix is shown in Fig. 8. Based on the low-resolution image acquired by presampling, a high-resolution image with the same resolution as the imaging target is first generated by bilinear interpolation, and then sparse transformation is carried out based on the sparse basis, which will be used in the image restoration process. Finally, the obtained coefficients are taken as the diagonal elements of the weight coefficient matrix after logarithmic operation.

4 Multiangle Image Restoration and Integration Strategy

From the corresponding relationship between the BCS model and the actual system described above, it can be seen that the 2-D image is integrated into a one-dimensional (1-D) vector for processing in the theoretical model, which raises an optimized selection of the signal integration method. When a 2-D image is integrated into a 1-D signal by row and column, respectively, there must be differences in the characteristics of the two signals. Therefore, for the same compressed sampling, if different signal integration methods are adopted in the image restoration process, that is, the same image is restored from multiple angles, then the multiple restored images can be fused to obtain a better image. However, it should be noted that this method achieves an improvement in the image quality at the cost of multiplying the restoration time.

The method of integrating a 2-D image into a 1-D vector includes: zig-zag integration by row, zig-zag integration by column, serpentine integration by row, serpentine integration by column, as shown in Fig. 9. Equations (4) and (5) in Sec. 2.2 are expressed in the form of zig-zag integration by row, and the other three integration methods are expressed as follows.

1. If the zig-zag integration by column is adopted, then the elements in the measurement matrix Φ^b can be organized as follows:

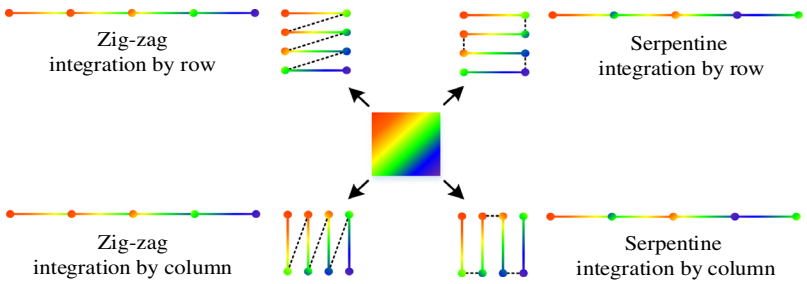

Fig. 9 The schematic diagram of multiangle integration strategy.

$$\Phi^b_{p,(j-1)\times r+i} = C(p)^b_{i,j} \qquad (i = 1\ldots r, j = 1\ldots c) \quad (p = 1\ldots m, b = 1\ldots B). \tag{13}$$

The elements in the signal matrix X^b to be measured are organized as follows:

$$X^b_{(j-1)\times r+i} = G^b_{i,j} \qquad (i = 1\ldots r, j = 1\ldots c). \tag{14}$$

2. If the serpentine integration by row is adopted, then the elements in the measurement matrix Φ^b can be organized as follows:

$$\begin{cases} \Phi^b_{p,(i-1)\times c+j} = C(p)^b_{i,j} & \text{when } i \text{ is odd} \\ \Phi^b_{p,(i-1)\times c+[c-(j-1)]} = C(p)^b_{i,j} & \text{when } i \text{ is even} \end{cases} \quad (i = 1\ldots r, j = 1\ldots c)(p = 1\ldots m, b = 1\ldots B). \tag{15}$$

The elements in the signal matrix X^b to be measured are organized as follows:

$$\begin{cases} X^b_{(i-1)\times c+j} = G^b_{i,j} & \text{when } i \text{ is odd} \\ X^b_{(i-1)\times c+[c-(j-1)]} = G^b_{i,j} & \text{when } i \text{ is even} \end{cases} \quad (i = 1\ldots r, j = 1\ldots c). \tag{16}$$

3. If the serpentine integration by column is adopted, then the elements in the measurement matrix Φ^b can be organized as follows:

$$\begin{cases} \Phi^b_{p,(j-1)\times r+i} = C(p)^b_{i,j} & \text{when } i \text{ is odd} \\ \Phi^b_{p,(j-1)\times r+[r-(i-1)]} = C(p)^b_{i,j} & \text{when } i \text{ is even} \end{cases} \quad (i = 1\ldots r, j = 1\ldots c)(p = 1\ldots m, b = 1\ldots B). \tag{17}$$

The elements in the signal matrix X^b to be measured are organized as follows:

$$\begin{cases} X^b_{(j-1)\times r+i} = G^b_{i,j} & \text{when } i \text{ is odd} \\ X^b_{(j-1)\times r+[r-(i-1)]} = G^b_{i,j} & \text{when } i \text{ is even} \end{cases} \quad (i = 1\ldots r, j = 1\ldots c). \tag{18}$$

The matrices processed by the above four signal integration methods are substituted into Eq. (2) for restoration, respectively, and then the restored 1-D signal is inversely integrated into a 2-D image. Further, the images obtained by the four methods are averaged to get the final restored image. The whole image restoration process is equivalent to performing four restorations for the same sampling, so the time consumed for image restoration is also increased by four times. Meanwhile, the proposed method does not affect the self-adaptive compressed sampling and image restoration described above and can be superimposed on the basis of the above method.

5 Path of Image Restoration

According to the proposed self-adaptive BCS imaging system and multiangle integrated image restoration method, this section combs the working path of image restoration process. In Fig. 10,

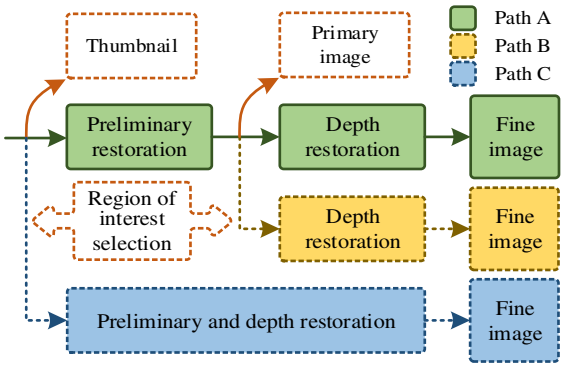

Fig. 10 The path of image restoration.

preliminary restoration refers to self-adaptive compressed sampling and image restoration, whereas depth restoration refers to superimposing multiangle integrated restoration method on the former.

The conventional image restoration and display process is shown in the path A of Fig. 10: the low-resolution thumbnail is directly displayed based on the presampled data, then the primary image is obtained by preliminary restoration, and finally the fine image is obtained by depth restoration. Alternatively, when the thumbnail is displayed, the region of interest can be selected artificially, and then preliminary and depth restoration are sequentially performed only for the local region, thereby improving the real-time performance, as shown in the path C of Fig. 10. It is also feasible to artificially select the region of interest when the primary image is displayed, and then perform depth restoration for the region, which shortens the image restoration time to some extent, as shown in the path B of Fig. 10.

6 Experimental Verification and Analysis

6.1 *Explanation of Experimental Parameters*

The resolution of the remote sensing image selected in the experiment is 512×512, and it is divided into 32×32 blocks by the BCS system, each of which has a size of 16×16. In the theoretical model, DCT is selected as the sparse transform base, random Bernoulli matrix is used as the measurement matrix due to the limitation of hardware implementation, and the orthogonal matching pursuit algorithm is applied for image restoration.

For the presampling stage in the sampling process, on the one hand, as many presampling times as possible are needed to extract more precise priori feature information, on the other hand, as few presampling times as possible are also necessary to reduce the impact on the whole sampling process. Considering the experimental parameters comprehensively, the presampling times of each block is set to 4. And the peak signal-to-noise ratio (PSNR) is used as the image quality evaluation criterion.

6.2 *Experimental Results of Self-Adaptive Compressed Sampling with Different Significant Information Maps*

The four remote sensing images selected in the experiment are shown in Fig. 11. The remarkable feature of remote sensing images is that the difference in the richness of information between regions is more obvious. Therefore, the advantages of the self-adaptive compressed sampling method proposed in this paper are more easily highlighted.

Taking the image remote 1 as an example, the saliency information maps generated by different algorithms based on the presampled data are shown in Fig. 12. It can be seen from this figure that all four algorithms can identify regions with rich information, but they are slightly different from each other.

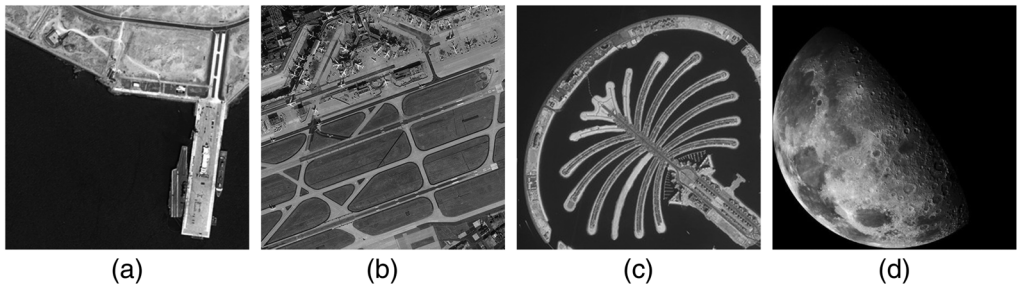

Fig. 11 The original target images: (a) remote 1, (b) remote 2, (c) remote 3, and (d) remote 4.

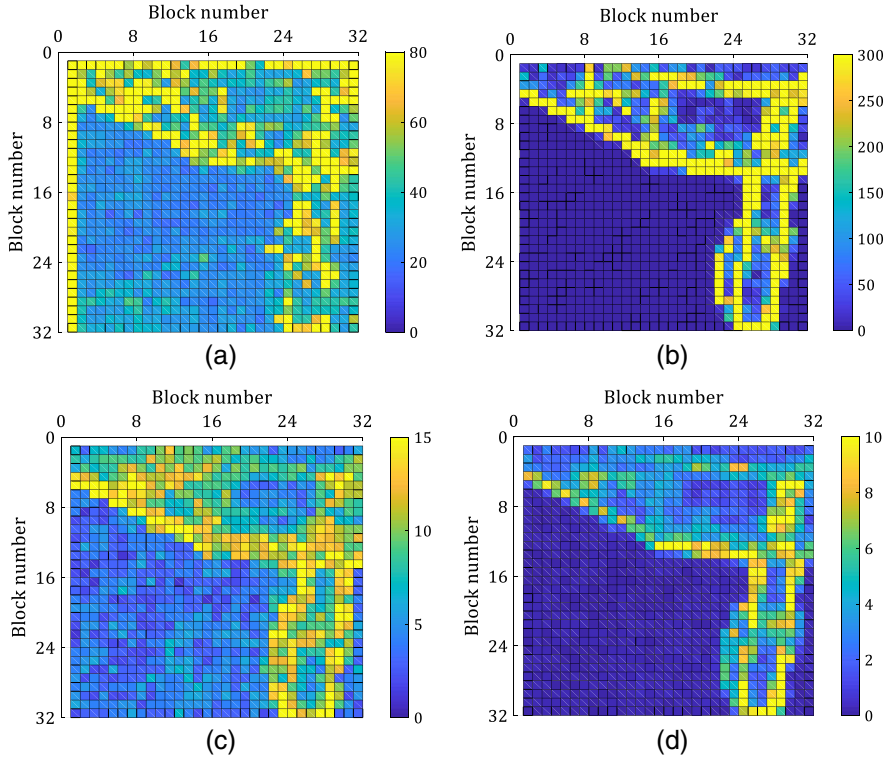

Fig. 12 The saliency information maps generated by different algorithms. (a) Sign function algorithm, (b) variance algorithm, (c) significant coefficient algorithm, and (d) texture feature algorithm.

Based on the above saliency information maps, the compressed sampling allocation strategy is then implemented to obtain the results of sampling ratio allocation, as shown in Fig. 13, wherein the system parameters are: the average sampling ratio D_a is 0.6, the initial minimum sampling ratio $D_{\min}$ is 0.4, and the maximum sampling ratio $D_{\max}$ is 0.95.

It can be seen from this figure that although the final results of sampling ratio allocation obtained by the four algorithms are different, the overall trend shows that higher sampling ratios are applied to the significant regions, which is in line with the expectation of the sampling ratio allocation strategy. Then the results of sampling ratio allocation shown in Fig. 13 are substituted into the theoretical model, and the restored images are shown in Fig. 14, in which the texture feature algorithm is intuitively optimal.

In order to further quantitatively compare the image quality under different saliency information map generation algorithms, the quality evaluation results of the restored images are recorded in Table 1. It can be seen from the table that compared with the traditional BCS method, the self-adaptive sampling method with different algorithms has achieved a better image quality, in which the quality of the restored image obtained by the texture feature algorithm is optimal. Therefore, the texture feature algorithm is selected as the saliency information map generation algorithm hereinafter.

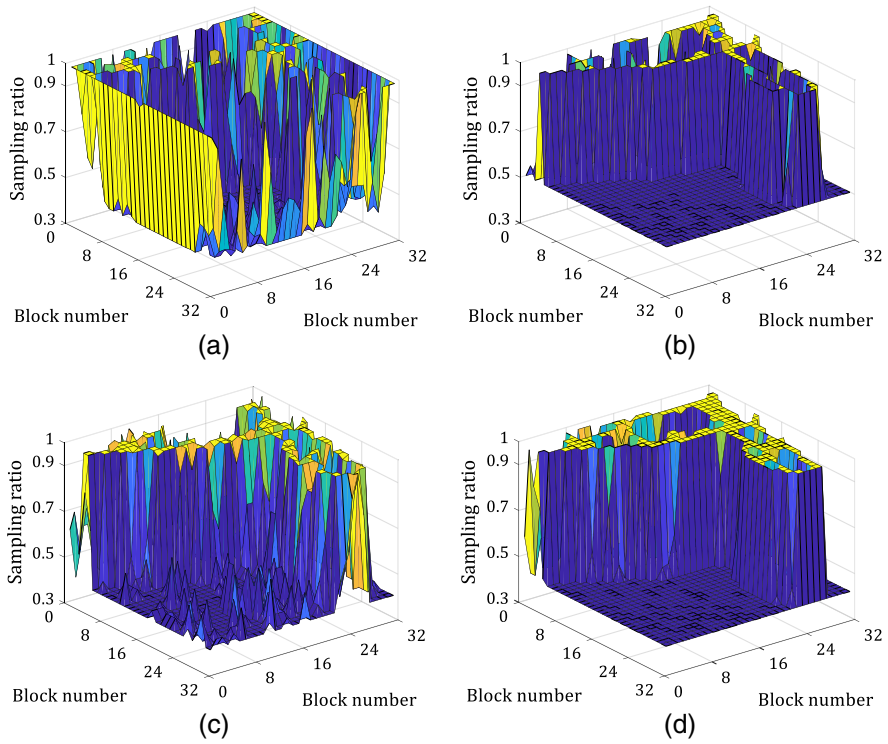

Fig. 13 The results of sampling ratio allocation for self-adaptive compressed sampling. (a) Sign function algorithm, (b) variance algorithm, (c) significant coefficient algorithm, and (d) texture feature algorithm.

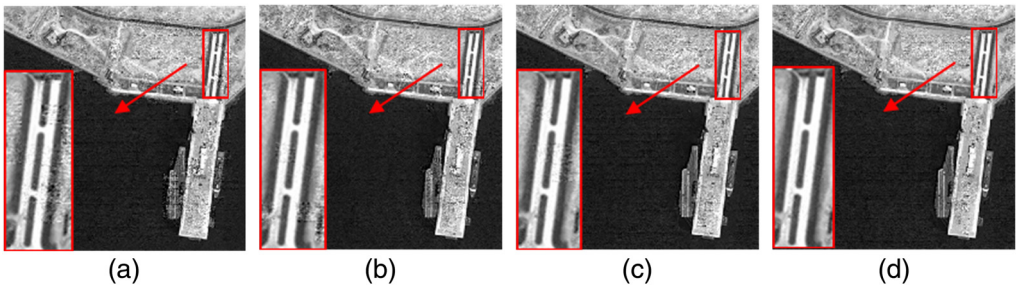

Fig. 14 The restored images obtained by self-adaptive compressed sampling method. (a) Sign function algorithm, (b) variance algorithm, (c) significant coefficient algorithm, and (d) texture feature algorithm.

Table 1 The quality evaluation results of the restored images with different saliency information map generation algorithms (unit: dB).

	Method				
Image	Traditional	Sign function	Variance	Significant coefficient	Texture feature
Remote1	24.20	25.10	25.23	26.30	26.78
Remote2	18.75	19.03	18.83	19.41	19.30
Remote3	22.15	22.65	22.43	23.29	23.67
Remote4	24.24	26.83	26.31	26.16	29.06

6.3 *Experimental Results of Combined Application of Self-Adaptive Compressed Sampling and Self-Adaptive Image Restoration*

In order to analyze the contribution of self-adaptive compressed sampling and self-adaptive image restoration to the improvement of restored images, the traditional BCS, self-adaptive compressed sampling (BCS-AS), self-adaptive image restoration (BCS-AR), and their combination (BCS-AS-AR) are adopted, respectively, for the same imaging target, and the quality evaluation results of restored images are shown in Table 2.

Figure 15 shows the relationship between PSNR of the restored images and sampling ratio under different combinations, which is drawn based on the data in Table 2. It can be seen from this figure that compared with the traditional BCS, both self-adaptive compressed sampling and self-adaptive image restoration can effectively improve the image quality. When self-adaptive compressed sampling is adopted alone, the improvement of the image quality becomes more significant with the increase of sampling ratio. When self-adaptive image restoration is adopted alone, the improvement of the image quality becomes less significant with the increase of sampling ratio, and the image quality is even lower than the traditional block-based method when the sampling ratio reaches 0.8. When both of them are adopted at the same time, the image quality is improved significantly in the case of low sampling ratio, whereas it is lower than either method alone in the case of high sampling ratio.

Based on the above results, it can be concluded that self-adaptive image restoration can significantly improve the image quality at low sampling ratio, whereas at high sampling ratio, it will

Table 2 The quality evaluation results of restored images under different combinations (unit: dB).

	Method			
Ratio	BCS	BCS-AS	BCS-AR	BCS-AS-AR
0.3	16.84	18.98	21.06	22.16
0.4	19.60	21.41	22.57	23.62
0.5	21.83	23.62	24.55	24.29
0.6	24.20	26.78	25.92	25.04
0.7	26.28	29.84	27.14	25.47
0.8	29.03	32.42	27.98	25.73

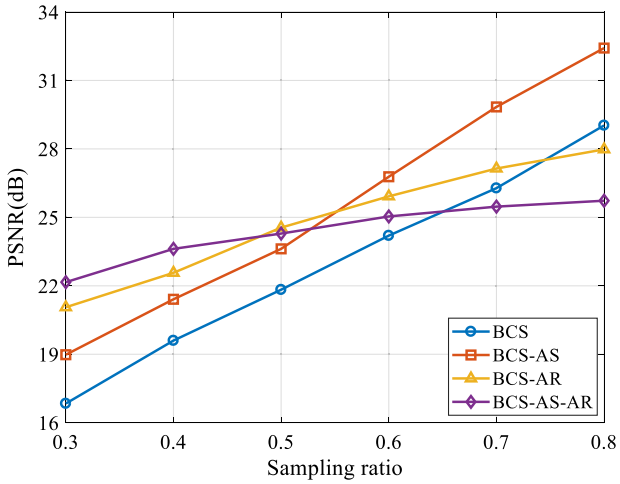

Fig. 15 The relationship between PSNR of the restored images and sampling ratio under different combinations.

result in image quality degradation. Therefore, it is necessary to propose an improved strategy to eliminate the negative effects of self-adaptive image restoration.

6.4 *Improved Strategy for Combined Application of Self-Adaptive Compressed Sampling and Self-Adaptive Image Restoration*

To solve the above problem, the basic principle of the improved strategy is: when self-adaptive compressed sampling and self-adaptive restoration are adopted simultaneously, selective processing is carried out between different blocks, and self-adaptive restoration is shielded for blocks with high sampling ratio. The specific implementation method is: the sampling ratio of each block is compared with the preset threshold D_{th} before image restoration. If it is higher than the threshold, then shielding self-adaptive restoration, otherwise no shielding. The quality evaluation results of restored images under different thresholds are recorded in Table 3.

Figure 16 shows the relationship between PSNR of the restored images and threshold D_{th} under different average sampling ratios, which is drawn based on the data in Table 3. It can be seen from this figure that the image quality first improves with the increase of threshold D_{th}, and then deteriorates sharply. The thresholds corresponding to a significant improvement of the image quality are different under various average sampling ratios. However, the PSNR of the restored image achieves the maximum when the threshold D_{th} is about 0.8 under all sampling ratios and drops sharply when approaching the maximum sampling ratio.

Table 3 The quality evaluation results of restored images under different thresholds (unit: dB).

	D_{th}								
D_a	1.0[a]	0.3	0.4	0.5	0.6	0.7	0.8	0.9	0.95
0.3	22.16	20.99	21.73	22.24	22.38	22.38	22.43	22.38	22.33
0.4	23.62	23.22	24.10	24.55	24.78	24.83	24.74	24.65	24.57
0.5	24.29	23.62	26.06	26.62	27.02	27.19	27.15	27.16	26.91
0.6	25.04	26.78	26.78	28.79	29.34	29.42	29.57	29.51	29.49
0.7	25.47	29.84	29.84	29.84	31.41	31.79	32.12	32.13	32.17
0.8	25.73	32.42	32.42	32.42	32.42	33.64	34.06	33.91	33.94

[a]It corresponds to the case of Sec. 6.3.

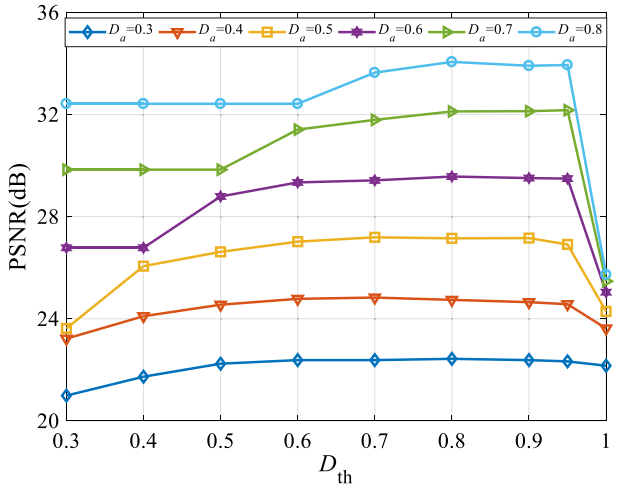

Fig. 16 The relationship between PSNR of the restored images and threshold D_{th} under different average sampling ratios.

Under the premise of lower threshold, the number of blocks adopting self-adaptive restoration increases with the increase of D_{th}, which is beneficial to image restoration, thus improving the image quality. Meanwhile, as the threshold increases, more and more blocks with high sampling ratio adopt self-adaptive restoration, and the negative effect of self-adaptive restoration gradually becomes prominent, resulting in a decline in the image quality. When the threshold D_{th} reaches 1, self-adaptive restoration will be adopted for all blocks, which corresponds to the case of Sec. 6.3. The phenomenon of sudden elevation and sudden descent of curves in Fig. 16 can be explained as follows. Taking the average sampling ratio $D_a = 0.6$ as an example, in which point the minimum sampling ratio is set to 0.4 and the maximum sampling ratio is set to 0.95. It can be seen from Fig. 13 that the blocks with the minimum sampling ratio and the maximum sampling ratio in the imaging target each occupy a higher proportion. Therefore, when the threshold is greater than the minimum sampling ratio of 0.4, a large number of blocks with the minimum sampling ratio are suddenly incorporated into the self-adaptive restoration range, so the image quality has a significant improvement. When the threshold is greater than the maximum sampling ratio of 0.95, a large number of blocks with the maximum sampling ratio are suddenly incorporated into the self-adaptive restoration range, which results in a sharp deterioration of the image quality. Considering comprehensively, the threshold D_{th} is set to 0.8 in the case of the current experimental parameters.

6.5 *Comparison of the Methods Proposed in this Paper with other Methods*

The multiangle image restoration strategy superimposed on the self-adaptive compressed sensing method proposed in this paper is defined as BCS-AS-AR-M, and the self-adaptive compressed sensing methods proposed in Refs. 39 and 40 are defined as BCS-method1 and BCS-method2, respectively. Then taking the image remote1 as the target, and the restored images obtained by the above two methods and the methods described in this paper are shown in Fig. 17 under the condition that the sampling ratio is 0.6.

In order to further quantitatively compare the image quality under different methods, the quality evaluation results of the restored images are recorded in Table 4, and they are also plotted in Fig. 18 for easy viewing.

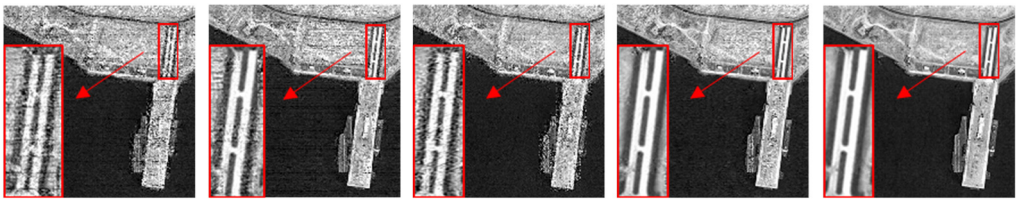

Fig. 17 The restored images obtained by different methods. (a) BCS, (b) BCS-method1, (c) BCS-method2, (d) BCS-AS-AR, and (e) BCS-AS-AR-M.

Table 4 The quality evaluation results of restored images obtained by different methods (unit: dB).

	Method				
Ratio	BCS	BCS-method1	BCS-method2	BCS-AS-AR	BCS-AR-AR-M
0.3	16.84	18.97	17.22	22.43	27.81
0.4	19.60	21.51	20.71	24.74	30.43
0.5	21.83	24.13	22.90	27.15	32.98
0.6	24.20	26.80	25.27	29.57	35.55
0.7	26.28	29.47	27.25	32.12	38.32
0.8	29.03	32.50	29.66	34.06	40.47

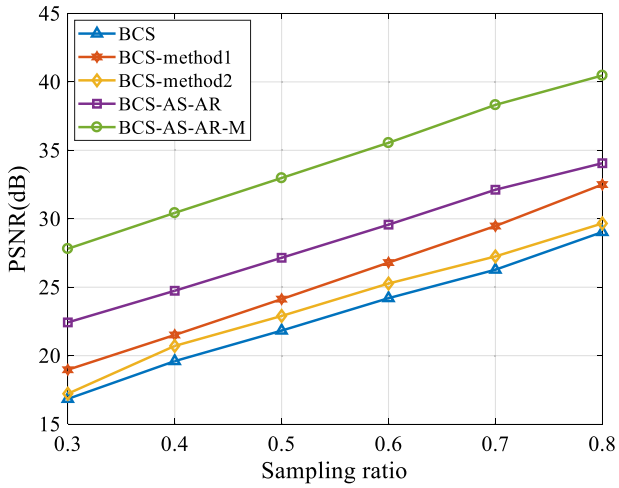

Fig. 18 The relationship between PSNR of the restored images and sampling ratio when different methods are adopted.

It can be seen from this figure that under all sampling ratios, there are always BCS-AS-AR-M better than BCS-AS-AR, BCS-AS-AR better than BCS-method1, BCS-method1 better than BCS-method2, and BCS-method2 better than BCS. This shows that compared with the traditional BCS, the methods proposed in Refs. 39 and 40 can effectively improve the image quality, and the image quality of the self-adaptive method proposed in this paper is better than the above two methods. Furthermore, compared with all the above methods, multiangle restoration strategy can greatly improve the image quality at the cost of multiplying the image restoration time.

For compressed sensing imaging systems, in addition to pursuing high-quality images, the real-time problem also needs to be considered, which is directly related to the computational complexity of image restoration algorithms. In order to quantify the impact of various imaging control strategies on the image restoration process, we intend to describe the complexity of the algorithm through the time consumed by simulation calculation. The image restoration time obtained by simulation calculation is recorded in Table 5.

Compared with traditional BCS, BCS-method1 does not introduce additional processing steps in the image restoration process. However, due to the difference in sampling ratio allocation, the overall computational complexity is increased, which leads to an increase in time consumption. Because the weight matrix used in image restoration is fixed rather than calculated in real time, the consumption time of BCS-method2 is basically the same as that of traditional BCS. For the proposed BCS-AS-AR method, it is not only to face the impact of the increase in computational complexity caused by the difference in sampling ratio allocation, but also to

Table 5 The image restoration time obtained by simulation calculation under different methods (unit: second)

	Method				
Ratio	BCS	BCS-method1	BCS-method2	BCS-AS-AR	BCS-AR-AR-M
0.3	11.72	20.68	11.67	23.02	93.61
0.4	25.91	46.85	25.83	49.72	201.29
0.5	46.60	77.40	47.44	78.81	322.92
0.6	77.51	111.91	79.75	114.30	465.67
0.7	118.75	151.34	124.97	160.24	649.31
0.8	187.51	207.60	191.06	210.02	853.21

provide time for the weight matrix generation, so the time consumption is slightly more than that of BCS-method1. The increased time is used to complete the weight matrix generation calculation, which is basically fixed about 3 s. It should be noted that the increase in image restoration time introduced by our method will gradually drown in the image restoration algorithm as the sampling ratio increases and the image size increases. Especially in the field of remote sensing, which is characterized by large-scale imaging, the disadvantage of imaging time is not obvious. In addition, the BCS-AS-AR-M method is equivalent to repeating the image restoration algorithm four times, so the time consumption in theory should be four times the previous method, which is indeed consistent with the results in Table 5.

7 Conclusions

Based on the significant differences between regions of remote sensing images, a self-adaptive BCS method is proposed in this paper. Compared with the traditional BCS system, the prior information of the imaging target is obtained first by adding presampling process. On the one hand, it is used to generate a saliency information map, which guides the reasonable allocation of self-adaptive sampling ratios between blocks in the compressed sampling process, thereby improving the sampling efficiency. On the other hand, it is used to generate the weighted sparse coefficient matrix, which will be substituted into the theoretical model in the image restoration process, thus improving the image restoration efficiency. The experimental results show that the imaging quality of the proposed method has a significant improvement compared with the traditional system and is also superior to several existing self-adaptive methods.

The method proposed in this paper improves the image quality significantly by optimizing the imaging strategy without affecting the hardware architecture of the traditional BCS system, which is instructive to the BCS for remote sensing applications.

Acknowledgments

This work was supported by the Strategic Priority Research Program of the Chinese Academy of Sciences (Grant No. XDA17010205). The authors would like to thank the reviewers for their constructive suggestions.

References

1. E. J. Candes, J. Romberg, and T. Tao, "Robust uncertainty principles: exact signal reconstruction from highly incomplete frequency information," *IEEE Trans. Inf. Theory* **52**, 489–509 (2006).
2. D. L. Donoho, "Compressed sensing," *IEEE Trans. Inf. Theory* **52**, 1289–1306 (2006).
3. R. G. Baraniuk, "Compressive sensing [lecture notes]," *IEEE Signal Process. Mag.* **24**, 118–121 (2007).
4. E. J. Candes and M. B. Wakin, "An introduction to compressive sampling," *IEEE Signal Process. Mag.* **25**, 21–30 (2008).
5. L. Carin, D. Liu, and B. Guo, "In situ compressive sensing," *Inverse Prob.* **24**, 015023 (2008).
6. J. A. Tropp et al., "Beyond Nyquist: efficient sampling of sparse bandlimited signals," *IEEE Trans. Inf. Theory* **56**, 520–544 (2010).
7. L. P. Yaroslavsky, "Compression, restoration, resampling, 'compressive sensing': fast transforms in digital imaging," *J. Opt.* **17**, 073001 (2015).
8. S. Qu et al., "Data compression and SNR enhancement with compressive sensing method in phase-sensitive OTDR," *Opt. Commun.* **433**, 97–103 (2019).
9. M. Haltmeier et al., "Compressed sensing and sparsity in photoacoustic tomography," *J. Opt.* **18**, 114004 (2016).
10. Y. Nan, Z. Yi, and C. Bingxia, "Review of compressed sensing for biomedical imaging," in *7th Int. Conf. Inf. Technol. Med. and Educ.*, pp. 225–228 (2015).

11. C. Graff and E. Sidky, "Compressive sensing in medical imaging," *Appl. Opt.* **54**, C23–C44 (2015).
12. X. Zhou et al., "Evaluation of imaging protocol for ECT based on CS image reconstruction algorithm," *Chin. Phys. C* **38**, 048201 (2014).
13. B. Li et al., "Mixed sparse representation for approximated observation-based compressed sensing radar imaging," *J. Appl. Remote Sens.* **12**, 035015 (2018).
14. X. Ren, L. Li, and E. Dang, "Compressive sampling and gated viewing three-dimensional laser radar," *J. Phys. Conf. Ser.* **276**, 012142 (2011).
15. Y. Zhang et al., "3D single-pixel video," *J. Opt.* **18**, 035203 (2016).
16. H. P. Babcock et al., "Fast compressed sensing analysis for super-resolution imaging using L1-homotopy," *Opt. Express* **21**, 28583–28596 (2013).
17. S. Zhang et al., "Fast frequency-domain compressed sensing analysis for high-density super-resolution imaging using orthogonal matching pursuit," *IEEE Photonics J.* **11**, 6900108 (2019).
18. J. Li and Z. Liu, "Efficient compressed imaging method for a microsatellite optical camera," *Appl. Opt.* **55**, 8070–8081 (2016).
19. T. Li et al., "Subsource-based compression in remote sensing," *J. Appl. Remote Sens.* **7**, 073555 (2013).
20. M. F. Duarte et al., "Single-pixel imaging via compressive sampling," *IEEE Signal Process. Mag.* **25**, 83–91 (2008).
21. A. C. Sankaranarayanan and A. Veeraraghavan, "Parallel compressive imaging," in *Comput. Opt. Sens. and Imaging* (2015).
22. J. P. Dumas et al., "Computational imaging with a highly parallel image-plane-coded architecture: challenges and solutions," *Opt. Express* **24**, 6145–6155 (2016).
23. I. Y. Chun and B. Adcock, "Compressed sensing and parallel acquisition," *IEEE Trans. Inf. Theory* **63**, 4860–4882 (2017).
24. L. Gan, "Block compressed sensing of natural images," in *15th Int. Conf. Digital Signal Process.*, pp. 403–406 (2007).
25. A. Adler et al., "Block-based compressed sensing of images via deep learning," in *IEEE 19th Int. Workshop on Multimedia Signal Processing (MMSP)*, pp. 1–6 (2017).
26. G. Coluccia, D. Valsesia, and E. Magli, "Smoothness-constrained image recovery from block-based random projections," in *IEEE 15th Int. Workshop Multimedia Signal Process.*, pp. 129–134 (2013).
27. H. Liu and W. Wang, "Block compressed sensing reconstruction with adaptive-thresholding projected Landweber for aerial imagery," *J. Appl. Remote Sens.* **9**, 095037 (2015).
28. H. Yang and X. Lin, "A novel variation-based block compressed sensing restoration method," *Proc. SPIE* **10806**, 108064K (2018).
29. B. Zhang et al., "Matrix permutation meets block compressed sensing," *J. Visual Commun. Image Represent.* **60**, 69–78 (2019).
30. Y. Zhou and H. Guo, "Collaborative block compressed sensing reconstruction with dual-domain sparse representation," *Inf. Sci.* **472**, 77–93 (2019).
31. H. Zheng and X. Zhu, "Sampling adaptive block compressed sensing reconstruction algorithm for images based on edge detection," *J. China Univ. Posts Telecommun.* **20**, 97–103 (2013).
32. W. Wang, W. Yang, and J. Li, "An adaptive sampling method of compressed sensing based on texture feature," *Optik* **127**, 648–654 (2016).
33. S. Zhu, B. Zeng, and M. Gabbouj, "Adaptive reweighted compressed sensing for image compression," in *IEEE Int. Symp. Circuits and Syst.*, pp. 1–4 (2014).
34. Y. Yang et al., "Reweighted compressive sampling for image compression," in *Picture Coding Symp.*, pp. 1–4 (2009).
35. Z. Gao et al., "Image representation using block compressive sensing for compression applications," *J. Visual Commun. Image Represent.* **24**, 885–894 (2013).
36. S. Zhu, B. Zeng, and M. Gabbouj, "Adaptive sampling for compressed sensing based image compression," *J. Visual Commun. Image Represent.* **30**, 94–105 (2015).
37. J. Xu et al., "Perceptual rate-distortion optimized image compression based on block compressive sensing," *J. Electron. Imaging* **25**, 053004 (2016).

38. X. Zhang et al., "Self-adaptive structured image sensing," *Opt. Eng.* **51**, 127001 (2012).
39. Y. Yu, B. Wang, and L. Zhang, "Saliency-based compressive sampling for image signals," *IEEE Signal Process. Lett.* **17**, 973–976 (2010).
40. Y. Yang et al., "Perceptual compressive sensing for image signals," in *IEEE Int. Conf. Multimedia and Expo*, pp. 89–92 (2009).

Biographies of the authors are not available.